Molecular evidence of Late Archean archaea and the presence of a subsurface hydrothermal biosphere

Gregory T. Ventura*†, Fabien Kenig*, Christopher M. Reddy‡, Juergen Schieber§, Glenn S. Frysinger¶, Robert K. Nelson‡, Etienne Dinel‖, Richard B. Gaines¶, and Philippe Schaeffer**

*Department of Earth and Environmental Sciences, University of Illinois at Chicago, M/C 186, 845 West Taylor Street, Chicago, IL 60607-7059; ‡Department of Marine Chemistry and Geochemistry, Woods Hole Oceanographic Institution, MS#4, Woods Hole, MA 02543-1543; §Department of Geological Sciences, Indiana University, 1001 East 10th Street, Bloomington, IN 47405-1405; ¶Department of Science, U.S. Coast Guard Academy, 310 Smith Hall, New London, CT 06320-8101; ‖Earth Sciences Department, Ottawa-Carleton Geoscience Centre, University of Ottawa, Ottawa, ON, Canada K1N 6N5; and **Laboratoire de Géochimie Bio-organique, Unité Mixte de Recherche 7509 du Centre National de la Recherche Scientifique, Ecole de Chimie, Polymères et Matériaux, Université Louis Pasteur, 25 Rue Becquerel, 67200 Strasbourg, France

Edited by John M. Hayes, Woods Hole Oceanographic Institution, Falmouth, MA, and approved July 20, 2007 (received for review December 13, 2006)

Highly cracked and isomerized archaeal lipids and bacterial lipids, structurally changed by thermal stress, are present in solvent extracts of 2,707- to 2,685-million-year-old (Ma) metasedimentary rocks from Timmins, ON, Canada. These lipids appear in conventional gas chromatograms as unresolved complex mixtures and include cyclic and acyclic biphytanes, C_{36}–C_{39} derivatives of the biphytanes, and C_{31}–C_{35} extended hopanes. Biphytane and extended hopanes are also found in high-pressure catalytic hydrogenation products released from solvent-extracted sediments, indicating that archaea and bacteria were present in Late Archean sedimentary environments. Postdepositional, hydrothermal gold mineralization and graphite precipitation occurred before metamorphism (≈2,665 Ma). Late Archean metamorphism significantly reduced the kerogen's adsorptive capacity and severely restricted sediment porosity, limiting the potential for post-Archean additions of organic matter to the samples. Argillites exposed to hydrothermal gold mineralization have disproportionately high concentrations of extractable archaeal and bacterial lipids relative to what is releasable from their respective high-pressure catalytic hydrogenation product and what is observed for argillites deposited away from these hydrothermal settings. The addition of these lipids to the sediments likely results from a Late Archean subsurface hydrothermal biosphere of archaea and bacteria.

An early evolution of archaea is supported by the discovery of ^{13}C-depleted methane in ≈3,500-million-year-old (Ma) hydrothermal fluid inclusions in cherts from the Pilbara Craton of Australia (1). In the Late Archean, archaea are likely to have played a dominant role in the global carbon cycle. Kerogens with $\delta^{13}C$ values down to −60‰ versus VPDB (Vienna Pee Dee belemnite) are common between 2,800 and 2,600 Ma (2, 3). These kerogens are considered to have been formed by the burial of methanotrophs or other organisms that assimilated ^{13}C-depleted carbon resulting from isotopic fractionations during methanogenesis (4). Biogenic methane not immediately assimilated is thought to have entered the atmosphere (5), enhanced greenhouse warming, and offset the reduced insolation from a "faint" young sun (6). As such, archaea were indirectly responsible for the existence of liquid water at the Earth's surface.

In more recent sediments, the presence of archaea is inferred from isotopic evidence of methane cycling (7, 8) or by detection of domain-specific membrane lipids such as glycerol dibiphytanyl glycerol tetraethers (GDGTs) (9) or their degradation products (10). The oldest known GDGTs (11) and biphytane-derived, C_{39} head-to-head isoprenoids (12) occur in Upper Jurassic sediments and in crude oil, respectively. The archaeal lipid crocetane was tentatively identified in 1,640-Ma sediments from the Barney Creek Formation (13).

In principle, it should be possible to extend this record. Petroleum fluid inclusions, bitumen globules, and pyrobitumens occur in 3,200- to 2,440-Ma black shales of the Pilbara Craton, Australia (14–16). Migrated hydrocarbons of Archean age have been identified in the Witwatersrand Basin of South Africa (17). Molecular fossils diagnostic of bacteria and eukarya have been extracted from 2,700-Ma sediments of the Hammersley Basin of Western Australia and provide direct evidence for a Late Archean existence of these two domains of life (18). Hydrothermal settings further may enhance the potential for Archean molecular fossils to survive because high-pressure and -temperature aqueous solutions suppress the thermal destruction of hydrocarbons (19).

This investigation was conducted to assess the abundance and preservation of molecular fossils within Late Archean hydrothermal environments and hydrothermally altered sediments. Samples were collected from the lower greenschist metasediments (20, 21) of the Tisdale and Porcupine Assemblage (≈2,707–2,685 Ma) from the southern Abitibi greenstone belt near Timmins, ON, Canada. Here we report the occurrence of hydrocarbon molecular fossils diagnostic of archaea and bacteria among the solvent-extractable lipids and high-pressure catalytic hydrogenation (HPCH) products (22) of these samples. We provide evidence that these lipids are of Archean age and that a portion of the organic matter trapped in these sediments was derived from a subsurface hydrothermal biosphere.

Results and Discussion

Thirty samples were collected from the core library of the Ministry of Northern Development and Mines (Toronto, ON), as well as from the Dome, Hoyle Pond, and Owl Creek mines located in the Porcupine Gold Camp (PGC), a gold mine district. These samples span the Vipond and Gold Center Formations of the upper Tisdale Assemblage (2,710–2,704 Ma) and the Krist and Hoyle Formation of the Porcupine Assemblage (2,690–2,685 Ma; Fig. 1) (23). The Vipond Formation volcanic rocks range in composition from mafic to intermediate and from tholeiitic basalt to tholeiitic dacite interbedded by interflow sedimentary rocks (24). Four different interflow sedimentary units of greywacke and carbonaceous argillites were analyzed. Two samples of carbonaceous interflow sediments were analyzed from the overlying Gold Center Formation. These sediments were deposited between mafic pillowed flows, pillow breccias, and flow breccias. One sample of a sheared, carbonaceous argillite from the Krist Formation was analyzed. The Krist Forma-

Author contributions: G.T.V. and F.K. designed research; G.T.V. performed research; F.K., C.M.R., J.S., G.S.F., R.K.N., R.B.G., and P.S. contributed new reagents/analytic tools; G.T.V., F.K., C.M.R., J.S., G.S.F., R.K.N., E.D., and P.S. analyzed data; and G.T.V. and F.K. wrote the paper.

The authors declare no conflict of interest.

This article is a PNAS Direct Submission.

Abbreviations: HPCH, high-pressure catalytic hydrogenation; PGC, Porcupine Gold Camp; TOC, total organic carbon; UCM, unresolved complex mixture; GC×GC, comprehensive two-dimensional gas chromatography.

†To whom correspondence should be addressed. E-mail: gventura@whoi.edu.

This article contains supporting information online at www.pnas.org/cgi/content/full/0610903104/DC1.

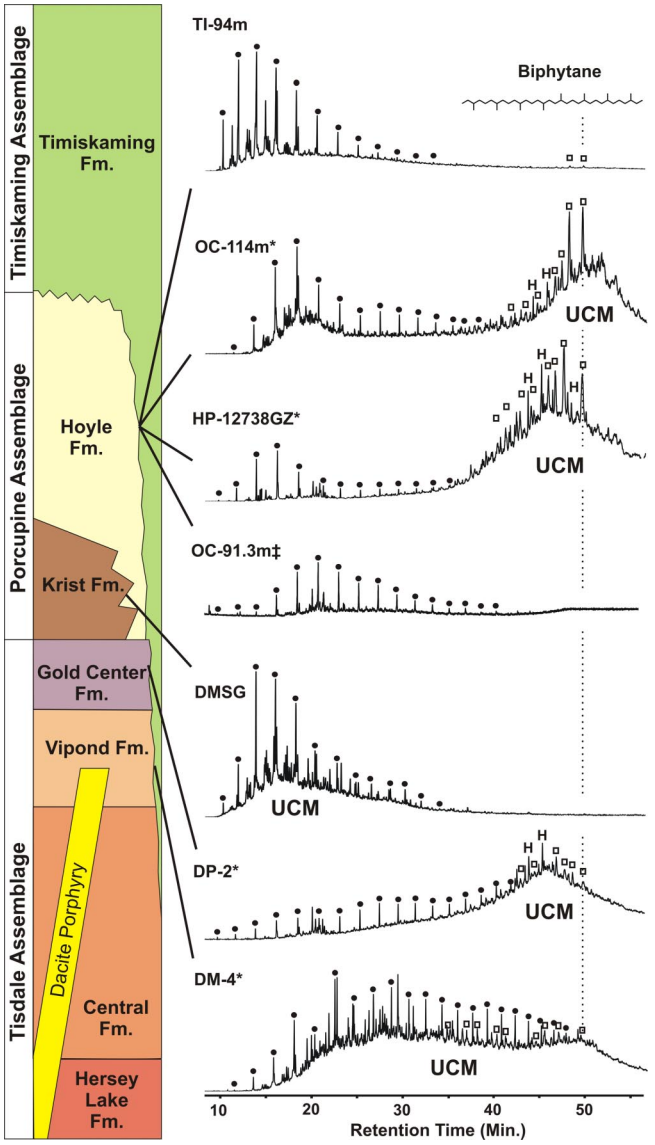

Fig. 1. Stratigraphic profile of the Timmins area (*Left*) and total ion current (TIC) chromatograms of samples (*Right*) illustrating differences in the hydrocarbon fractions of each formation. *, Samples collected in areas of gold mineralization; ‡, Hoyle Formation basalt unit; ●, *n*-alkanes; H, hopanes; □, biphytane and its derivatives.

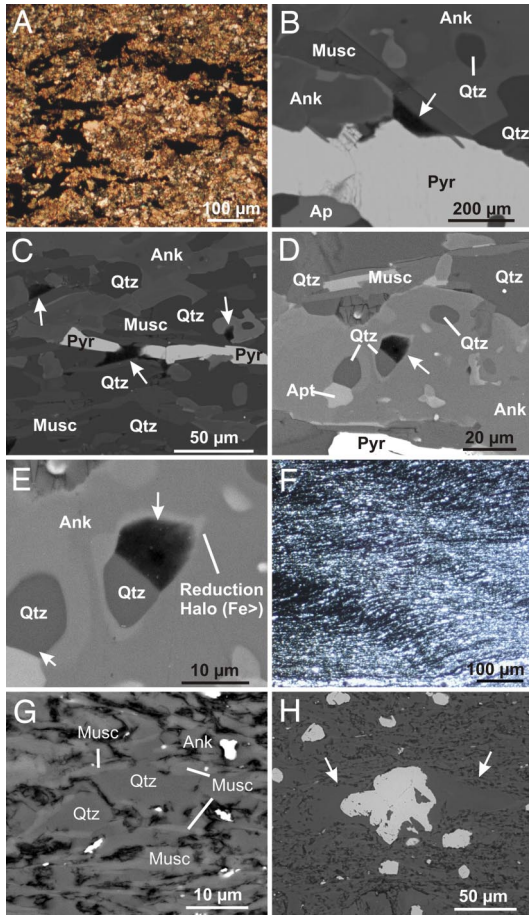

Fig. 2. SEM images of polished thin sections (30- and 100-μm) of Late Archean metasediments. (*A*) Transmitted light photomicrograph of the Vipond Formation greywacke sample DM-1. Opaque areas are sulfide minerals. (*B* and *C*) SEM backscatter images of carbon-rich inclusions (arrows). (*D*) Sample DM-1 SEM backscatter image of a carbon-rich inclusion (arrows) in Fe-dolomite. (*E*) Close-up of the carbon-rich inclusion. An Fe-enriched reduction halo surrounds the partially quartz-filled inclusion. (*F*) Transmitted light photomicrograph of the Hoyle Formation argillite sample OC-114m. Original sedimentary lamination inclined 30° with horizontal slaty cleavage. (*G*) SEM backscatter image of Hoyle Formation sample OC-110m with carbon-rich films filling the interstices of quartz, muscovite, and Fe-dolomite grains. (*H*) Quartz-filled pressure shadows (arrows) flanking sulfide minerals. Apt, apatite; FD, Fe-dolomite; Musc, muscovite; Qtz, quartz; Pyr, pyrite.

tion is dominated by subaerially deposited calc-alkaline felsic pyroclastic volcanic rocks (24). Nineteen core samples were collected from argillites and wackes of the Hoyle Formation, which consists of turbidites interbedded between basalt flows on the distal, deeper-water margin of a submarine fan system (25). Two of these samples occupied "gray zones," which are volcanic breccia enriched in graphite, pyrite, dolomite, and ferroan-dolomite precipitated by hydrothermal gold-bearing fluids (26). Gray zones cross-cut volcanic rock, argillaceous turbidites, and interflow sedimentary units. Additionally, four interbedded basalt flows were sampled to monitor postdepositional alteration and contamination. The Porcupine Assemblage is unconformably topped by fault-controlled, clastic sediments of the Timiskaming Sequence that range from 2,676 to 2,670 Ma (27). No other sedimentary units are known from this area. By 2,670 ± 7 Ma, the Porcupine Assemblage was a site of hydrothermal gold mineralization (28). The PGC was metamorphosed at 200–300°C between 2,669 and 2,665 Ma (20, 21, 29).

Polished 30- and 100-μm thin sections were analyzed by SEM. The Vipond Formation samples contain wavy-laminar, carbon-rich films adjacent to sedimentary sulfides [Fig. 2*A*; supporting information (SI) *Text*]. Additionally, carbon-rich inclusions were identified within these greywackes. These inclusions occur as fillings in ≈1-μm wide cracks between and adjacent to pyrite grains (Fig. 2 *B* and *C*); as ≈10- to 20-μm diameter, rounded inclusions within the interstices of occluded quartz grains (Fig. 2*C*); and as ≈10- to 20-μm diameter, rounded, carbon-rich inclusions within secondary mineral phases such as ferroan-dolomite (Fig. 2 *D* and *E*). The large (≈100- to 300-μm) ferroan-dolomite grains formed during precipitation of minerals from hydrothermal fluids (30) and contain rounded inclusions of apatite and quartz. Iron-enriched halos surrounding quartz and carbon-rich inclusions (Fig. 2 *D* and *E*) indicate that these spaces likely were filled by a hydrocarbon-bearing fluid that later became solid bitumen before quartz deposition.

The fine-grained, metasedimentary fabric of samples from the Hoyle Formation contains laminae with carbon-rich films that

Table 1. Mass yields, TOC, and $\delta^{13}C$

Sample name	Mass, g*	Bit, mg†	s/u HC, ppm‡	Aro, ppm§	TOC, wt%¶	C, g‖	H/C**	$\delta^{13}C_{VPDB}$, ‰††
Hoyle Formation								
TI-94m	141.93	49.0	23.3	2.1	2.0	2.8	0.020	−39.1
TI-117.8m	130.82	12.0	0.3	15.3	0.9	1.2	0.019	−31.7
TI-82.5m	120.28	16.0	34.9	15.8	0.8	1.0	0.087	−33.7
TI-83m	134.84	10.0	17.1	4.4	1.8	2.4	0.128	−33.7
TI-275.14m	63.08	30.0	28.5	46.0	5.1	3.2	0.003	−42.0
TI-52m	95.81	37.0	4.2	1.0	3.7	3.5	0.012	−36.6
TI-180m	130.81	1.0	0.3	24.5	1.1	1.4	0.029	−29.7
TI-603m	109.37	4.0	7.3	2.7	0.4	0.4	0.041	−29.2
TI-39.25m	131.58	7.0	0.8	2.3	0.4	0.5	0.006	−21.5
TI-128.75m	123.66	1.0	0.8	1.6	0.2	0.2	Nm	−20.9
OC1–114m	104.08	16.0	2.9	0.4	9.3	4.7	0.005	−28.7
OC1–118m	157.91	8.0	0.3	0.3	4.5	7.1	0.005	−28.5
OC1–116.5m	43.27	4.0	18.5	4.6	4.6	2.0	0.000	−33.7
OC1–161.7m	75.37	24.0	13.3	91.5	4.9	3.7	0.000	−31.6
OC-89m	121.06	3.0	8.3	0.8	1.2	1.5	0.011	−25.4
OC-110.8m	51.37	3.0	77.9	1.9	7.4	3.8	0.000	−34.8
HP12687	42.07	1.0	28.5	0.4	1.0	0.4	0.003	−19.5
Grey Zone samples								
HP12738 GZ	61.59	1.0	28.5	4.8	1.2	0.6	0.007	−37.2
HPGZ-2	89.51	0.6	6.5	4.9	Nm	Nm	Nm	Nm
Basalt units								
OC-91.3m	41.0	0.2	4.9	Nm	Nm	Nm	Nm	Nm
OC-49.2m	63.57	0.5	3.1	Nm	Nm	Nm	Nm	Nm
OC-147.5m	52.59	0.15	1.9	Nm	Nm	Nm	Nm	Nm
OC-153m	61.13	0.2	3.3	Nm	Nm	Nm	Nm	Nm
Krist Formation								
DMGS	161.5	10.0	8.7	1.9	1.7	2.8	0.013	−20.9
Gold Center Formation								
DP-1	143.33	10.0	0.2	0.2	0.4	0.5	0.035	−16
DP-2	99.06	1.0	0.04	0.04	0.1	0.1	0.013	−15.1
Vipond Formation								
DM-1	173.43	5.0	0.2	0.2	0.6	1.1	0.021	−15.7
DM–2	127.18	25.0	0.9	0.4	0.5	0.7	0.008	−32.5
DM–3	183.83	1.0	0.3	0.04	0.1	0.1	0.040	−27.3
DM–4	158.84	6.0	0.2	0.1	0.1	0.1	0.000	−28.8

Nm, parameter not measured.
*Mass of ground rock powder used in solvent extraction.
†Mass of extracted bitumen.
‡Parts per million (ppm) hydrocarbon fraction calculated 1 μg of hydrocarbons per gram of rock powder.
§Aromatic hydrocarbon fractions in parts ppm.
¶TOC measured as weight percentage of kerogen per mass of extracted rock powder.
‖Grams of carbon is mass of solvent-extracted rock powder multiplied by TOC.
**Hydrogen/carbon ratio of the kerogen.
††Carbon isotopic values versus VPDB in ‰ notation from nonextracted rock powder.

contain bitumen and kerogen (Fig. 2 *F* and *G*). No carbon-rich inclusions were observed. Many of the fine-grained matrix sulfides are flanked by quartz-filled pressure shadows (Fig. 2*H*), suggesting the remobilization of quartz during prograde metamorphism. In all stratigraphic sections, the initial sediment porosity was occluded by remobilized quartz and by the growth of potassium and aluminum silicate (Fig. 2*H*). Conversion to slate resulted in the formation of dense, nonporous rock that is impermeable to postmetamorphic fluids and/or migrating oils. There is no evidence of post-Archean remineralization or retrograde metamorphic alteration that could trap more recent contributions of organic matter.

Organic Carbon and Graphite. All PGC samples have hydrogen-to-carbon (H/C) ratios <0.2 (Table 1). Hoyle Formation samples collected from areas of gold mineralization have near-zero H/C ratios (Table 1). The coexistence of saturated hydrocarbons and nearly graphitic kerogen could suggest a postmetamorphic addition of hydrogen-rich organic compounds. However, if factors other than thermal stress influence the concentrations of hydrogen and carbon of sedimentary organic matter, then H/C ratios are not a reliable proxy of hydrocarbon preservation.

The PGC experienced extensive carbonatization before metamorphism (Fig. 3) (30). Fluid with high CO_2 fugacity induced precipitation of carbonates in less reducing settings (31) and graphite in more reducing environments. Exogenous additions of graphite are common in the PGC gold centers (24) and globally observed in hydrothermal load-gold deposits (32–34). Additions of graphite,

$$n\ CO_{2\ (mantle)} + (2n + x)\ CH_2 \rightarrow 3n\ C^0 + 2n\ H_2O + x\ CH_{2\ (hydrothermally\ altered)}$$

(rather than generation of graphite *in situ* by dehydrogenation and aromatization of kerogen), can explain the coexistence of hydrocarbons with kerogens having near-zero H/C ratios. The addition of hydrothermal graphite also accounts for the slightly more positive values of $\delta^{13}C_{ker}$ of Hoyle Formation samples collected in areas of gold mineralization and the lack of correlation among H/C ratios, total organic carbon (TOC), and bitumen extracted from the PGC sediments (Table 1).

Biphytanes in Bitumens. The solvent-extractable hydrocarbons of these powdered sediment samples were analyzed by gas chroma-

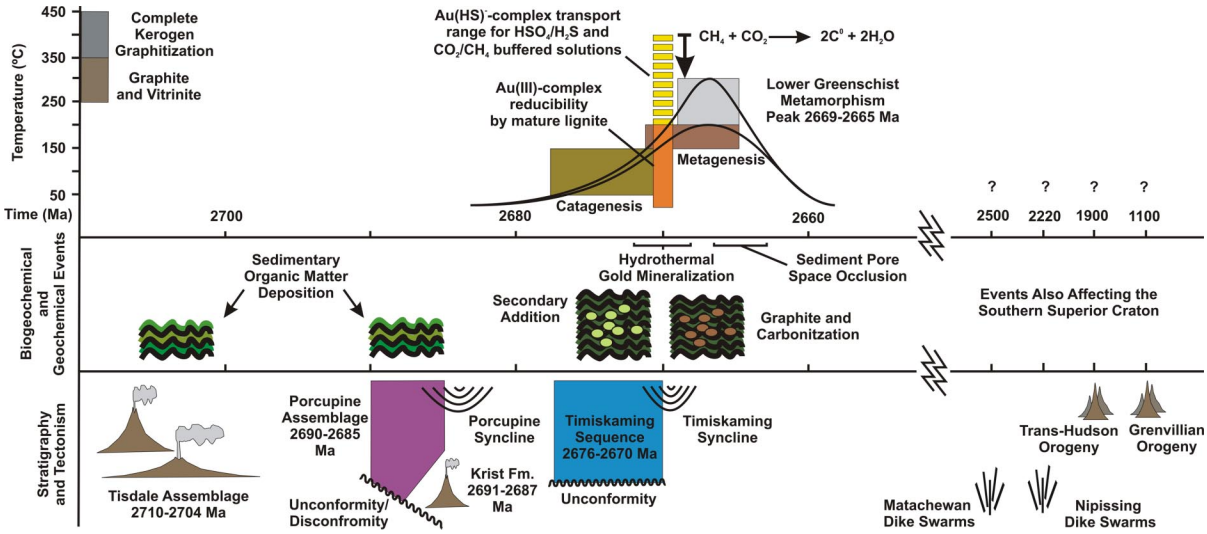

Fig. 3. Time sequence of geological and geochemical events affecting the Porcupine Gold Complex modified from ref. 54. Overlain on the hypothesized burial temperature curve are the temperature ranges of gold solubility (55), reduction of Au onto lignite (56), catagenesis and metagenesis (57), kerogen conversion to graphite (58), and stability of graphite in mixtures of CO_2 and CH_4 (59).

tography mass spectrometry (GCMS) (*SI Text*). All but one sample contains biphytane and C_{36}–C_{39} irregular isoprenoids derived from biphytane (Fig. 1). These compounds were identified from their mass spectra and by coinjection with a standard containing acyclic, mono-, bi-, and tricyclic biphytanes (SI Fig. 6). The abundances of biphytanes relative to other extractable compounds vary between and within formations. Hoyle Formation samples located away from gold mineralization centers have low concentrations of biphytanes and extended hopanes. In contrast, those compounds and their degradation products are among the most abundant compounds in the solvent-extractable hydrocarbons of samples collected in areas of gold mineralization (Fig. 1). Only the sample of the Krist Formation does not contain archaeal lipids.

Archaeal Lipids of Unresolved Complex Mixtures (UCMs). Gas chromatograms of hydrocarbon extracts of samples collected in areas of gold mineralization display discrete peaks of biphytane and related degradation products that elute within a pronounced UCM (Fig. 1). Bacterial biomarkers such as C_{27}–C_{35} hopanoid hydrocarbons and eukaryotic biomarkers such as C_{27}–C_{29} steroids were identifiable by GCMS, but most of the constituents the UCMs remain undetermined.

Comprehensive two-dimensional GC coupled to a time-of-flight mass spectrometer (GC×GC-TOFMS) was used to resolve and identify the components forming the UCMs of the Hoyle Formation (*SI Text*) (Fig. 1). As shown in Fig. 4, the constituents of the UCM are separated into bands of peaks with different retention times in the second dimension. The constituents of the first band are C_{36}–C_{41} head-to-head acyclic isoprenoids, including biphytane. The second, third, and fourth bands include, respectively, mono-, bi-, and tricyclic biphytane and their derivatives (C_{36}–C_{39}). Tetracyclic triterpenoids (steroids) and pentacyclic triterpenoids (hopanoids) form a fifth and a sixth band in the second dimension.

The C_{40} mono-, bi-, and tricyclic biphytane derivatives and their lower C_{36}–C_{39} pseudohomologues each form doublets, triplets, and at least quadruplets of peaks (Fig. 4), respectively, with identical mass spectra. In contrast, each of the C_{36}–C_{40} acyclic isoprenoids forms a single peak. With time and thermal stress, acyclic and cyclic biphytanes (35, 36) isomerize at methyl-substituted chiral carbons on the isoprenoid chain (37) and at alkyl-substituted chiral carbon of pentacyclic rings. Although diastereomers formed by isomerization of acyclic compounds cannot be resolved with the GC×GC columns used (38), the doublets, triplets, and quadruplets observed for the cyclic compounds probably represent mixtures of diastereomers.

To date, the isomerization rate of such compounds under thermal stress is unknown. Although isomerization of acyclic isoprenoids is well established, a pattern of cyclic-isoprenoid diastereomers like that in the PGC samples has not been previously reported. The formation of such diastereomers must be favored by high temperatures and potentially requires the addition of metal catalysts (39) or exogenous sources of hydrogen to expand the activation energy range for isomerization without excessive hydrocarbon cracking (19). Such conditions might be common to hydrothermal environments where serpentinization and the hydrolytic disproportionation of H_2O forms solutions with high H_2 fugacity (19, 40, 41).

Potential for Bitumen Contamination. Sedimentary organic matter can be contaminated by postburial addition of hydrocarbons. Potential sources include drilling fluids, laboratory processing, migration of oils, and infiltration by meteoric groundwater. Solvent washes of the core exterior contain abundant contaminants. Accordingly, the surfaces of cores were ground away before extraction. Solvent washes conducted after the removal of the core surface contain only trace concentrations of the same hydrocarbons extracted from the powdered sediments (*SI Text*). Because these differ compositionally from the surface contaminants, we believe they do not derive from laboratory or field contamination. Analytical blanks from solvent extraction and liquid chromatography have hydrocarbon contents 100 times smaller than those obtained from samples. In marked contrast to the significant differences between samples, replicate extraction of splits of a single sample yielded essentially identical mixtures of hydrocarbons. Solvent extracts of Hoyle Formation basalt units interstratifying the archaeal-rich turbidites do not contain archaeal lipids. However, these igneous rocks do have traces of hydrocarbons such as *n*-alkanes, pristane, and phytane (Fig. 1) attributable to rough storage and contamination by drilling fluids (*SI Text*).

The extractable hydrocarbons are unlikely to result from the migration of younger oils. The Vipond and Krist Formation samples were collected in ≈3-m-thick interflow deposits buried ≈800 m beneath successive mafic flows within the Dome Mine. Hydrocarbon mixtures extracted from the Vipond and Krist Formations differ from those extracted from the Hoyle Formation. With allowance for the higher temperatures experienced at the PGC, the

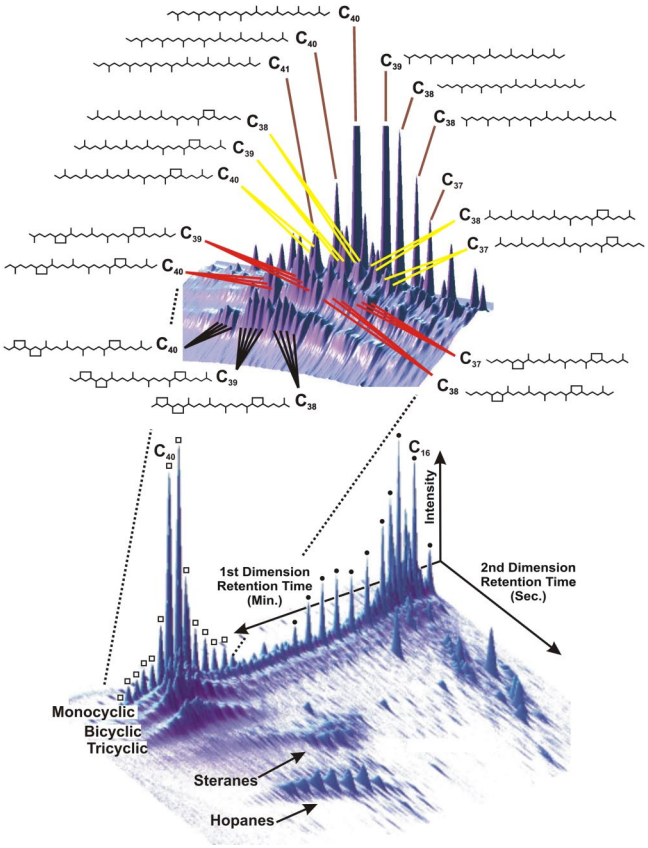

Fig. 4. Three-dimensional GC×GC-flame ionization detector chromatograms of the solvent extract from sample OC-114m of the Hoyle Formation. (*Lower*) Complete chromatograph. (*Upper*) Enlargement of region with archaeal lipids. Multiple peaks joined to a single molecular structure are diastereomers. ●, *n*-alkanes; □, irregular acyclic isoprenoids.

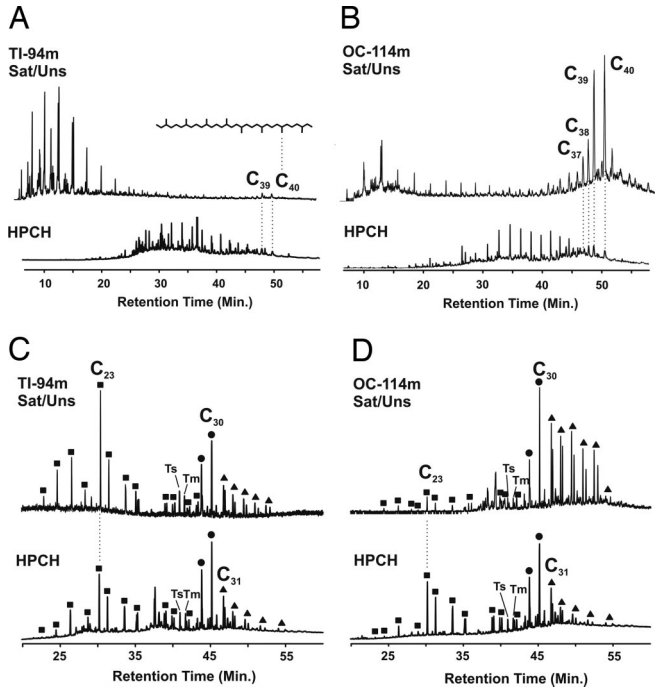

Fig. 5. Chromatograms illustrating contrasts between unmineralized (TI-94m, *Left*) and mineralized (OC-114m, *Right*) samples. Sat/Uns, hydrocarbon fraction of solvent extract. (*A* and *B*) Selected-ion chromatogram for mass to charge ratio (*m/z*) = 127, representing acyclic isoprenoids of archaeal origin. (*C* and *D*) Selected-ion chromatograms for *m/z* = 191, representing tricyclic and pentacyclic terpanes of bacterial origin. ■, Tricyclic terpanes; ●, C_{29} and C_{30} 17α(H), 21β(H) hopanes; ▲, C_{31} to C_{35} extended hopanes.

extracts of the Vipond and Krist Formations resemble those of younger hydrothermal settings, and the extracts of the Hoyle Formation samples resemble those of younger shelf sediments (42, 43). In contrast, even though the depositional environment of the Gold Center Formation is similar to that of the Vipond and Krist Formations, its extracts have hydrocarbon abundances and diversities comparable to those from the overlying Hoyle Formation (Fig. 1) (*SI Text*). Migration from older units is not possible because these units are entirely igneous. Accordingly, the hydrocarbons may derive in part from the postdepositional addition of Late Archean oil migrated from source rocks in the Hoyle Formation. For further information, see *SI Text*, SI Tables 2–5, SI Figs. 6–9, and SI Movie 1.

HPCH. The presence of archaeal- and bacterial-related lipid carbon skeletons in nonextractable organic matter is a strong indication that the lipids were part of the original sedimentary organic matter. HPCH can release lipid carbon skeletons from kerogen (44) and/or sulfides (22) trapped in metamorphosed sediments. Biphytane and C_{37}–C_{39} biphytane derivatives were observed in the HPCH products of all solvent-extracted sediment samples that contain extractable archaeal lipids (Fig. 5). Additionally, all HPCH products contain diasteranes, tricyclic terpanes, and thermally altered steranes and hopanes. Several HPCH products have diasterane/sterane, sterane/hopanes, and tricyclic terpane/hopanes ratios that differ from those of their corresponding extracts, indicating these lipids likely were cracked from the kerogen (SI Table 3). However, the HPCH products of some samples include *n*-alkanes, monomethyl- and monoethyl-branched alkanes, and cycloalkanes with carbon-number predominance that likely is indicative of contamination during storage (45).

HPCH products also can derive from incomplete sediment extraction, molecules that are adsorbed on kerogen, and/or intercalated bitumen. Because reextracted sediments yielded only extremely low abundances of lower-molecular-weight *n*-alkanes and elemental sulfur, we exclude incomplete extraction. Adsorption mainly occurs during early diagenesis and decreases substantially with increasing thermal maturity because of the loss of reactive sites on the kerogen (46). The PGC kerogens reached a thermal stress corresponding to the onset of metamorphism in the Late Archean (*SI Text*), and sediment porosity was significantly restricted thereafter. Any surviving, adsorbed organic matter, therefore, is Archean. The HPCH products also may contain intercalated bitumen, which forms by the entrapment of bitumen in the kerogen during the continued heating of a thermally mature kerogen (47). Such constituents must be intimately associated with the kerogen and, thus, also date from the Late Archean.

Second Addition of Archaeal and Bacterial Lipids. The presence of biphytane, steranes, and hopanes in the HPCH products indicates that all three domains of life were present in the Late Archean environment. However, the relative abundance of archaeal and bacterial products varies widely between samples. Specifically, archaeal and bacterial products are more abundant in sediments affected by gold mineralization (Fig. 5). Chromatograms in Fig. 5 *Left* and *Right* represent unmineralized and mineralized areas, respectively. Similar relative abundances of these compounds in geographically and temporally separated turbidites of the Porcupine Formation suggest consistent sources, low in archaeal biomass, during sediment deposition (Fig. 5 *A* and *C*). The abundance patterns of biphytane, biphytane derivatives, and C_{31}–C_{35} extended hopanes are similar in both the solvent extracts and HPCH products

of samples collected away from gold mineralization centers. In these samples, the biphytane concentration in bitumen typically is low and uncorrelated to the sediment's TOC (Table 1). In contrast, within gold mineralization centers, biphytane and the C_{39} derivative of biphytane often are the most abundant molecular fossils in the solvent extracts and correlate positively with TOC. The relative abundances of biphytane, biphytane derivatives, and C_{31}–C_{35} extended hopanes in the solvent extracts are much greater than in the HPCH products of the corresponding samples (Fig. 5). Additionally, several samples with low TOC, such as the hydrothermally altered "gray zone" and samples DP-1 and DP-2, have relatively high concentrations of biphytane and extended hopanes (*SI Text*), indicating that these lipids are unlikely to derive from cracking of kerogen and instead suggesting a secondary input of organic compounds.

Postmetamorphic hydrothermal activity is not likely to account for the secondary addition of organic matter. In the Southern Superior Province, it is linked to the 2,500-Ma Matachewan and 2,220-Ma Nipissing dyke swarms, the TransHudson orogeny (≈1,900 Ma), Kapuskasing uplift (1,900 Ma), and the Grenvillian Orogen (≈1,100 Ma), which involved tectonic pumping of fluids in reactivated Archean fault systems (48) (Fig. 3). These fluids would have traveled ≈100 kilometers before reaching the PGC. If such fluids added the archaeal biomarkers, then the basalt flows interstratifying the Hoyle Formation turbidites also would have been affected.

Alternatively, geochemical process relating to PGC gold mineralization may be responsible for variations in archaeal and bacterial lipid extract yields (Fig. 3). Gold is thought to have been transported within dilute, aqueous, carbonic fluids with low chlorine and high sulfur contents in the form of Au–HS^- complexes (49). Ore fluids were acidic (pH 5–6), and their redox properties were controlled by HSO_4/H_2S and CO_2/CH_4 mixtures at temperatures between 200–420°C (48). Based on the solubility of Au–$(HS)^-$, gold precipitation is thought to have occurred at cooler temperatures and/or lower pressure (49). The envelope of cooled, high sulfur and reduced, carbon-rich fluids surrounding this region of high heat flow would provide favorable conditions for hyperthermophilic communities of archaea and bacteria (50, 51). Continued burial likely would convert a subsurface biosphere's biomass into the observed secondary addition of hydrocarbons (Fig. 3).

Conclusions

A bacterial and archaeal subsurface biosphere now is believed to have a near-global extent, being found in marine sediments; in the fractures and vents near midoceanic spreading centers; within older, cooled basaltic crust beneath the oceans; in deep aquifers of basalts and granitic batholiths; and in deep oil reservoirs of continental settings (51–53). Our results provide molecular fossil evidence for the existence of archaea in Late Archean sedimentary environments and in subsurface hydrothermal settings. Considering the extent and composition of today's deep biosphere, it is likely that such hydrothermal subsurface communities have existed for much of Earth's history.

Materials and Methods

Sediments were extracted in DCM:MeOH (7.5:1, vol/vol) for 72 hr. Extracts were separated by liquid column chromatography. HPCH using 20 or 40 g of extracted sediment, 2 g of 5% rhodium on activated carbon, and 300 ml of 1,4-dioxane:H_2O (1:1, vol/vol) was done under pressure above 1,250 psi for 5 hr at 200°C. Extraction, separation, HPCH protocols, and instrumentation techniques are provided in *SI Text*.

We thank Porcupine Joint Venture and the Ministry of Northern Mines and Development (ON, Canada). We also thank Eric Barr and the late Richard Keele for their help with sampling; Roger Summons and Emmanuelle Grosjean (Massachusetts Institute of Technology, Cambridge, MA) and Neil Sturchio and Linnea Heraty (University of Illinois at Chicago) for sample analysis; Ben Van Mooy and Helen Fredricks (Woods Hole Oceanographic Institution) for use of an internal standard; and John Hayes (Woods Hole Oceanographic Institution) for invaluable editorial input. This project was supported by National Aeronautics and Space Administration Exobiology Grant NAG5-s13446 (to F.K.). SEM analysis was supported by National Science Foundation (NSF) Grant EAR 0318769 (to J.S.). GC×GC analysis was supported by NSF Grant IIS-0430835 and the Seaver Foundation (to C.M.R.).

1. Ueno Y, Yamada K, Yoshida N, Maruyama S, Isozaki Y (2006) *Nature* 440:516–519.
2. Schidlowski M, Hayes JM, Kaplan IR (1983) in *Earth's Earliest Biosphere: Its Origin and Evolution*, ed Schopf JW (Princeton Univ Press, Princeton), pp 149–186.
3. Eigenbrode JL, Freeman KH (2006) *Proc Natl Acad Sci* 103:15759–15764.
4. Hayes JM (1994) in *Nobel Symposium 84: Early Life on Earth*, ed Bengtsen S (Columbia Univ Press, New York).
5. Kasting JF (2005) *Precambian Res* 137:119–129.
6. Sagan C, Mullen G (1972) *Science* 177:52–56.
7. Collister JW, Summons RE, Lichtfouse E, Hayes JM (1991) *Org Geochem* 19:265–276.
8. Dix GR, Thomson ML, Longstaffe FJ, McNutt RH (1995) *Precambrian Res* 70:253–268.
9. De Rosa M, Gambacorta A (1988) *Prog Lipid Res* 27:153–175.
10. Chappe B, Michaelis W, Albrecht P (1979) in *Advances in Organic Geochemistry*, eds Douglas AG, Maxwell JR (Pergamon, Oxford), pp 265–274.
11. Carrillo-Hernandez TS, Adam P, Albrecht P, Derenne S, Largeau C (2001) in *21st International Meeting on Organic Geochemistry* (Krakow, Poland), p 78.
12. Petrov AA, Vorobyova NS, Zemskova ZK (1990) *Adv Org Geochem* 16:1001–1005.
13. Greenwood PF, Summons RE (2003) *Org Geochem* 34:1211–1222.
14. Buick R, Rasmussen B, Krapez B (1998) *AAPG Bull* 82:50–69.
15. Rasmussen B (2005) *Geology* 33:497–500.
16. Dutkiewicz A, Rasmussen B, Buick R (1998) *Nature* 395:885–888.
17. Spangenberg JE, Frimmel HE (2001) *Chem Geol* 173:339–335.
18. Brocks JJ, Logan GA, Buick R, Summons RE (1999) *Science* 285:1033–1036.
19. Lewan MD (1997) *Geochim Cosmochim Acta* 61:3691–3723.
20. Jolly WT (1978) in *Metamorphism in the Canadian Shield*, ed Fraser JA, Heywood WW (Geological Survey of Canada, Ottawa), Paper 78-10, pp 63–78.
21. Dimroth E, Imreh L, Rocheleau M, Goulet N (1982) *Can J Earth Sci* 19:1729–1758.
22. Mycke B, Michaelis W, Degens ET (1988) *Org Geochem* 13:619–625.
23. Ayer JA, Ketchum JWF, Trowell NF (2002) in *Summary of Field Work and Other Activities* (Ontario Geological Survey, ON, Canada), pp 5-1–5-16.
24. Brisbin DI (1997) *Geological Setting of Gold Deposits in the Porcupine Gold Camp, Timmins, Ontario* (Queen's University, Kingston, ON, Canada), p 611.
25. Born P (1995) *A Sedimentary Basin Analysis of the Abitibi Greenstone Belt in the Timmins Area, Northern Ontario, Canada* (Carleton University, Ottawa), p 489.
26. Heaman LM (1997) *Geology* 25:299–302.
27. Corfu F, Jackson SL, Sutcliffe RH (1991) *Can J Earth Sci* 28:489–503.
28. Bateman R, Ayer JA, Barr E, Dubé B, Hamilton MA (2004) in *Discover Abitibi Initiative: Ontario Geological Survey* (Queen's Printer for Ontario, Toronto), Open File Report 6145, p 90.
29. Thompson PH (2005) in *Discover Abitibi Initiative: Ontario Geological Survey* (Queen's Printer for Ontario, Toronto), Open File Report 6162, pp 1–104.
30. Fyon JA, Crocket JH, Schwarcz HP (1983) *J Geochem Explor* 18:245–266.
31. Veizer J, Hoefs J, Ridler RH, Jensen LS, Lowe DR (1989) *Geochim Cosmochim Acta* 53:845–857.
32. Gao ZL, Kwak TAP (1997) *J Geochem Explor* 59:259–274.
33. Craw D (2002) *Chem Geol* 191:257–275.
34. Jedwab J, Boulegue J (1984) *Nature* 310:41–43.
35. Sinninghe Damsté JS, Schouten S, Hopmans EC, van Duin ACT, Geenevasen JAJ (2002) *J Lipid Res* 43:1641–1651.
36. Montenegro E, Gabler B, Paradies G, Seemann M, Helmchen G (2003) *Angew Chem Int Ed* 42:2419–2421.
37. Maxwell JR, Cox RE, Eglinton G, Pillinger GT, Ackman RG, Hopper SN (1973) *Geochim Cosmoshim Acta* 37:297–313.
38. Patience RL, Rowland SJ, Mawxell JR (1978) *Geochim Cosmochim Acta* 42:1871–1875.
39. Akhmedov VM, Al-Khowaiter SH, Akhmedov E, Sadikhov A (1999) *Appl Catal A Gen* 181:51–61.
40. Seewald JS (1994) *Nature* 370:285–287.
41. Price LC, DeWitt E (2001) *Geochim Cosmochim Acta* 65:3791–3826.
42. Summons RE, Brassel SC, Eglinton G, Evans E, Horodyski RJ, Robins N, Ward DM (1988) *Geochim Cosmochim Acta* 52:2625–2637.
43. Simoneit BRT, Lein AY, Peresypkin VI, Osipov (2004) *Geochim Cosmochim Acta* 68:2275–2294.
44. Mycke B, Michaelis W, eds (1986) *Molecular Fossils from Chemical Degradation of Macromolecular Organic Matter* (Pergamon, Oxford).
45. Grosjean E, Logan GA (2007) *Org Geochem* 38:853–869.
46. Oehler JH (1977) *Precam Res* 4:221–227.
47. Behar F, Vandenbroucke M (1987) *Adv Org Geochem* 13:927–938.
48. Kerrich R, Ludden J (2000) *Can J Earth Sci* 37:135–164.
49. Loucks RR, Mavrogenes JA (1999) *Science* 284:2159–2163.
50. Huber R, Huber H, Stetter KO (2000) *Fems Microbiol Rev* 24:615–623.
51. Amend JP, Shock EL (2001) *FEMS Microbio Rev* 25:175–243.
52. Pedersen K (2000) *FEMS Microbiol Lett* 185:9–16.
53. Wellsbury P, Mather I, Parkes RJ (2002) *FEMS Microbiol Eco* 42:59–70.
54. Bleeker W (1999) *Econ Geol Monogr* 10:71–122.
55. Stefánsson A, Seward TM (2003) *Geochim Cosmochim Acta* 67:1677–1688.
56. Gatellier J-P, Disnar J-R (1989) *Adv Org Geochem* 16:631–640.
57. Peters KE, Walters CC, Moldowan JM (2005) *The Biomarker Guide* (Cambridge Univ Press, Cambridge, UK).
58. Diessel CFK, Brothers RN, Black PM (1978) *Contrib Mineral Petrol* 68:63–78.
59. Holloway JR (1984) *Geology* 12:455–458.